Available online at www.sciencedirect.com
SCIENCE DIRECT®
Journal of Chromatography A, 1033 (2004) 229–239
JOURNAL OF CHROMATOGRAPHY A
www.elsevier.com/locate/chroma

Optimizing control of simulated moving beds—linear isotherm

Stefanie Abel [a], Gültekin Erdem [b], Marco Mazzotti [a,*], Manfred Morari [b], Massimo Morbidelli [c]

[a] *Institute of Process Engineering, ETH Swiss Federal Institute of Technology Zurich, 8092 Zurich, Switzerland*
[b] *Automatic Control Laboratory, ETH Swiss Federal Institute of Technology Zurich, 8092 Zurich, Switzerland*
[c] *Institute for Chemical and Bio-Engineering, ETH Swiss Federal Institute of Technology Zurich, 8093 Zurich, Switzerland*

Received 2 April 2003; received in revised form 21 October 2003; accepted 23 January 2004

Abstract

A new optimization based adaptive control strategy for simulated moving beds (SMBs) is proposed. A linearized reduced order model, which accounts for the periodic nature of the SMB process, is used for online optimization and control. The manipulated variables are the four inlet flow rates, the outputs are the raffinate and extract concentrations. Concentration measurements at the raffinate and extract outlets are used as the feedback information. The state estimate from the periodic Kalman filter is used for the prediction of the outlet concentrations over a chosen horizon. Predicted outlet concentrations are the basis for the calculation of the optimal input adjustments, which maximize the productivity and minimize the desorbent consumption subject to constraints on product purities. The realization of this concept is discussed and the implementation on a virtual eight column SMB platform is assessed, in the case of binary linear systems. For a whole series of typical plant disturbances it is shown that the proposed approach is effective in minimizing off-spec products and in achieving optimal SMB operation, also in the case where there are significant model uncertainties.

Keywords: Simulated moving beds; Linear isotherms; Repetitive model predictive control

1. Introduction

The interest of the fine chemical and pharmaceutical industry for chromatographic separation technologies such as the simulated moving bed (SMB) has been increasing during the last decade [1–4]. Recently, new SMB schemes like the VARICOL process [5], multi-component separations and gradient applications [6,7], which require more information for design purposes, are also in focus. Such interest is due to the possibility of running a continuous process, that can achieve higher productivities with lower solvent consumption than the traditional batch process. This implies that the products are less diluted, which results in an easier and cheaper product recovery step. SMB technology attracts interest in particular in the field of enantioseparation, e.g. for enantiopure drug development, since it is a technique best suited for a two-cut fractionation of the feed stream, and it can be used at all scales of the development of a new drug, from the early tests to production.

The SMB concept is that of a continuous chromatographic countercurrent process (true moving bed (TMB)), where the liquid phase flows in the opposite direction of the solid phase. The key idea of an SMB is to simulate the solid phase motion of the corresponding TMB unit by using standard fixed bed chromatographic columns and periodically switching the inlet and outlet ports of the unit in the same direction as the fluid flow. As a result SMB technology not only profits from the counter-current contact between stationary and mobile phases, but also overcomes the difficulties connected with the movement of the solid phase in a TMB unit. The most widely adopted SMB scheme has four sections, as shown in Fig. 1. Each of them plays a specific role. With reference to the separation of a binary mixture, the feed stream is introduced between Sections 2 and 3, where the separation takes place. The less adsorbable component B is carried by the mobile phase and collected in the raffinate stream. On the other hand, the more adsorbable component A is retained by the solid phase and eluted in the extract stream. Component B is adsorbed in section 4, so the eluent is regenerated

* Corresponding author. Present address: Sonneggstrasse 3, CH-8092 Zurich, Switzerland. Tel.: +41-1-632-2456; fax: +41-1-632-1141
E-mail address: mazzotti@ipe.mavt.ethz.ch (M. Mazzotti).

0021-9673/$ – see front matter © 2004 Elsevier B.V. All rights reserved.
doi:10.1016/j.chroma.2004.01.049

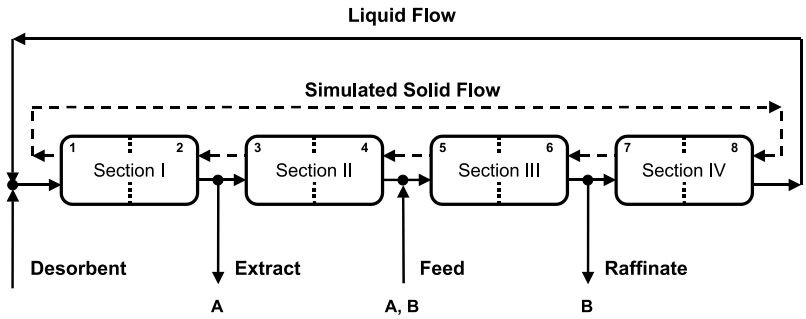

Fig. 1. Scheme of a simulated moving bed (SMB) unit.

and, after mixing with fresh eluent, recycled to section 1, where the solid adsorbent is regenerated. Each section of the SMB unit can consist of several fixed bed columns in order to closely approximate the continuous counter-current movement of the solid phase in the TMB unit.

Contrary to true countercurrent processes such as the TMB, SMB does not reach a steady state with constant profiles of all the process variables. Its stationary regime is a cyclic steady state where the concentration profiles along the unit move in the direction of the liquid flow. To simulate the solid movement, the inlet and outlet ports are switched periodically by one column position in the direction of the fluid flow. With respect to the inlet and outlet ports, the concentration profiles shift at each switch by one column position in the direction of the simulated solid movement. As a result, SMB units repeat the same time dependent behavior during each time period between two successive switches of the inlet and outlet ports, and, contrary to the TMB unit, modelling an SMB unit even in the stationary regime requires a time dependent model.

SMB separations are designed using models of different complexity. On the one hand, the Triangle Theory approach can be used, which is based on a local equilibrium model that accounts for competitive adsorption thermodynamics, but neglects column efficiency effects [8]. The advantages of this approach are: easy selection of near-optimal operating conditions based on simple algebraic computations, straightforward analysis of feed composition effects, thorough understanding of how flow rate changes affect separation performance, and the possibility of gaining a good understanding of SMB behavior, which is most useful when developing a new separation. On the other hand, detailed SMB models accounting for column efficiencies are best suited to find the best compromise between separation performance, e.g. productivity, eluent consumption, product purities and separation robustness [9].

How good the choice of the optimal operating conditions made by either approach is depends on the accuracy of the model parameters used in the model. Particularly the adsorption isotherms play a key role, due to their importance in determining the separation performance and to the intrinsic difficulty of their measurement. An additional issue in SMB operation is related to the fact that the unit is rather sensitive to a number of disturbances, e.g. feed composition or temperature changes, when it is operated close to its optimal operating conditions in terms of productivity and solvent consumption, and the stationary phase may undergo aging processes of a chemical and mechanical nature. It is a common practice to keep the operating point of the SMB at a reasonable distance from these optimal operating conditions in order to guarantee a certain level of robustness. In this case, since the SMB chromatography is a slow process, the unit can be controlled manually by the operator to keep the product specifications. On the other hand, the need for feedback control schemes becomes critical when the SMB units are operated at their optimal operating conditions. Therefore, there is a need to develop a closed-loop control system, which is capable on the one hand of controlling the SMB unit at the desired operating conditions, and on the other hand, of adapting the operating conditions to achieve the best possible separation and to fulfill the process specifications regardless of the disturbances that might occur. Such a control strategy would exploit the full economical potential of the SMB technology. Developing an automatic control concept for an SMB unit is a challenge not only due to its non-steady-state, non-linear, mixed continuous and discrete (the inlet-outlet switches) nature, but also due to the strong lag times that characterize the response to most disturbances. There are a few control approaches in the literature that have been proposed recently. One of them is based on the principle of asymptotically exact input/output-linearization [10,11]; the controller is based on a nonlinear state estimator using the TMB model. In another one, a model based SMB control is suggested where an optimal trajectory calculated off-line should be followed [12]; the optimal operating trajectories are recalculated and the local controllers are re-synthesized to account for the changes in the system characteristics. Another recently proposed approach makes use of nonlinear wave propagation phenomena and aims to control the two central sections of the SMB unit provided that the regeneration of the solid and liquid phases is guaranteed [13]. The bottle neck of these approaches is the requirement of precise physical data of the system and this would be a significant limitation especially in the case of SMBs applied to systems characterized by nonlinear isotherms. We believe that the SMB control strategy should be based on a small

amount of information from basic system characterization measurements. It can be extended and applied easily for SMBs operating under overloaded conditions, i.e. characterized by nonlinear adsorption isotherms, without any need of precise system characterization, which already poses itself as a difficult issue. In addition, the control concept should be able to handle multi-variable dynamics with time delays and hard constraints both on the process inputs and the states in a general manner. Model predictive control (MPC) has been proven to be the most effective control strategy for this type of problems [14,15] and will be applied in this work along the lines of what was proposed recently in the literature [16,17], i.e. the so-called repetitive model predictive control (RMPC) combining the concepts of MPC and repetitive control (RC).

2. SMB model

Let us consider a four-section, closed-loop SMB comprising various chromatographic columns of volume $V = LA$, where L and A are the column length and the cross-section, respectively. Each section j, (j = I, II, III, IV), has a volume V_j, which is V multiplied by the number of columns in section j. For the sake of simplicity, but without loss of generality, all examples in this work will refer to an eight column SMB with two columns per section, i.e. a 2-2-2-2 configuration where $V_j = 2V$. We will also limit the analysis to linear adsorption equilibria, but allow for column-to-column variability by considering different values of the total packing porosity ε_h in the h-th column, $h = 1, \ldots, 8$, that can differ from the nominal value ε. Each chromatographic column is modelled using the equilibrium dispersive model (see the Section 6 for the meaning of the symbols):

$$\varepsilon_h \frac{\partial c_{i,h}}{\partial t} + (1-\varepsilon_h)\frac{\partial q^*_{i,h}}{\partial t} + v_h \frac{\partial c_{i,h}}{\partial z} = \varepsilon_h D_i \frac{\partial^2 c_{i,h}}{\partial z^2} \quad (1)$$

$$q^*_{i,h} = H_i c_{i,h} \quad (i = \mathrm{A}, \mathrm{B};\ h = 1, \ldots, 8), \quad (2)$$

In the equations above v_h is the superficial velocity, which is the same for the columns belonging to the same section, i.e. $v_1 = v_2 = Q_\mathrm{I}/A$, $v_3 = v_4 = Q_\mathrm{II}/A$, $v_5 = v_6 = Q_\mathrm{III}/A$ and $v_7 = v_8 = Q_\mathrm{IV}/A$ for the 2-2-2-2 configuration. Proper boundary conditions (enforcing the inlet/outlet switching mechanism), proper initial conditions, and the following node balances complete the mathematical model (where $Q_h^{\mathrm{I/O}}$ identifies the inlet or outlet stream entering or leaving the SMB loop just before column h):

$$v_1 = v_8 + \frac{Q_1^{\mathrm{I/O}}}{A} \quad (3)$$

$$v_1 c_{i,1}^{in} = v_8 c_{i,8}^{\mathrm{out}} + \frac{Q_1^{\mathrm{I/O}}}{A} c_{i,1}^{\mathrm{I/O}} \quad (4)$$

$$v_{h+1} = v_h + \frac{Q_{h+1}^{\mathrm{I/O}}}{A}, \qquad (h = 1, \ldots, 7) \quad (5)$$

Table 1
Summary of system parameters for the base case

	L (cm)	A (cm^2)	ε	t^* (s)	N_p	H_A	H_B
Base case	10	1	0.7	480	100	4	2

$$v_{h+1} c_{i,h+1}^{in} = v_h c_{i,h}^{\mathrm{out}} + \frac{Q_{h+1}^{\mathrm{I/O}}}{A} c_{i,h+1}^{\mathrm{I/O}}, \quad (h = 1, \ldots, 7) \quad (6)$$

The SMB configuration in Fig. 1 corresponds to the following specifications: $Q_h^{\mathrm{I/O}} = 0$, for $h = 2, 4, 6, 8$; $Q_1^{\mathrm{I/O}} = Q_\mathrm{D}$; $Q_3^{\mathrm{I/O}} = -Q_\mathrm{E}$; $Q_5^{\mathrm{I/O}} = Q_\mathrm{F}$; $Q_7^{\mathrm{I/O}} = -Q_\mathrm{R}$. Moreover, we have $c_{i,1}^{\mathrm{I/O}} = c_i^D$; $c_{i,3}^{\mathrm{I/O}} = c_{i,2}^{\mathrm{out}}$; $c_{i,5}^{\mathrm{I/O}} = c_i^F$; $c_{i,7}^{\mathrm{I/O}} = c_{i,6}^{\mathrm{out}}$, where $c_{i,h}^{\mathrm{out}}$ is the concentration of component i at the outlet of column h. All the column dead volumes are assumed to be negligible.

All the computations in this work refer to a base case where the model parameters summarized in Table 1 are used. Axial dispersion is such that each column with respect to each solute corresponds to 100 theoretical stages, whereas differences among columns due to packing heterogeneity and velocity variations are neglected. The retention behavior of the two components to be separated is characterized by their Henry's constants in Eq. (2).

In implementing the model, axial dispersion, i.e. the right hand side of Eq. (1), will be accounted for through numerical dispersion, as discussed elsewhere [9,18]. It is worth noting that the equilibrium dispersive model is regarded as a good compromise between model accuracy and computational efficiency. The SMB mathematical model presented in this section has been used as a virtual plant in this work, and will be referred to simply as SMB plant in the following. Though the adsorption isotherm is linear, the SMB model is nonlinear due to the presence of the convective terms in Eqs. (1), (4) and (6).

3. SMB control

The wish of SMB users is to run an SMB separation where, regardless of the external disturbances, extract and raffinate have constantly the desired properties, e.g. product purity and concentration, while throughput, i.e. the amount of feed processed, is maximized, eluent consumption is minimized, and at the same time process constraints, e.g. maximum pressure drop due to pump limitations or to avoid leakage or damage of the column packing, are fulfilled. Ideally, this should be achieved having only limited information about the system's internal parameters, e.g. the adsorption isotherm that may be difficult to measure or may change during operation due to aging of the packing, and about the state of the system, that can be monitored through appropriate on-line detectors. RMPC is based on the idea that possible model prediction errors and the effect of period-invariant disturbances can be compensated using the measurements of the plant outputs. In essence, as sketched in Fig. 2, RMPC

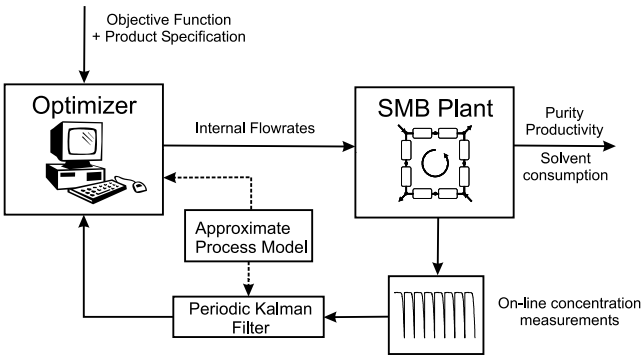

Fig. 2. Scheme of the optimizing control concept.

makes use of an approximate process model to predict the future evolution from the present state of the process. Using these results and the knowledge of the state of the system, the optimizer selects the set of inputs, i.e. the manipulated variables, that allows for the achievement of process specifications and optimal performance.

In the practical implementation a number of problems must be overcome. First, the detailed SMB model presented in Section 2 is nonlinear, and its solution requires significant computational time. Such a model leads to a nonlinear on-line optimization, which is computationally demanding. This implies that a simplified model of the plant must be used. Next, the state of the system is not easily accessible experimentally. Therefore, it has to be estimated by combining the information coming from the model and the available on-line measurements, e.g. the extract and raffinate compositions in our case. Filtering is needed to account for both the noise in the experimental measurements and for model inaccuracy, and a periodical Kalman filter is best suited for this purpose.

A summary of the features of the proposed control system is reported in the following. A more detailed description will be provided elsewhere [19]. In our approach, the manipulated variables are the four internal SMB flow rates, i.e. Q_{I}, Q_{II}, Q_{III} and Q_{IV}, which are adjusted by acting on Q_{I} itself and on the external flow rates Q_{E}, Q_{F} and Q_{R}. RMPC requires a predefined process period, therefore the switch time is not used as a manipulated variable, and is kept unchanged during SMB operation. It is worth noting that changing Q_j ($j = \mathrm{I, II, III, IV}$) affects in a linear manner the value of the corresponding flow rate ratio m_j:

$$m_j = \frac{Q_j t^* - V\varepsilon}{V(1-\varepsilon)}, \quad (j = \mathrm{I, II, III, IV}) \tag{7}$$

and these are the key variables in determining SMB performance as can be seen easily in the frame of triangle theory.

3.1. Simplified SMB model

A simplified SMB model which captures the most important dynamics of the process is derived in the following, starting from the detailed model introduced in Section 2.

First, the detailed SMB model is used to simulate the cyclic steady state behavior of the plant operated at a reference operating point. In this work, the flow rate ratios $m_{\mathrm{I}}^{\mathrm{ref}} = 4.0$, $m_{\mathrm{II}}^{\mathrm{ref}} = 2.1$, $m_{\mathrm{III}}^{\mathrm{ref}} = 3.9$ and $m_{\mathrm{IV}}^{\mathrm{ref}} = 2.1$ have been selected as the reference values, with t^*, V as indicated above. The column-to-column variations are unavoidable and not easy to measure precisely, hence it is preferable to have a controller based on only an average porosity value for the columns constituting the SMB unit. Therefore, the nominal porosity value is assigned for each column, i.e. $\varepsilon = 0.7$. The column-to-column variations are considered as a part of the uncertainties that should challenge the controller. The reference operating point is within the complete separation region in the $(m_{\mathrm{II}}, m_{\mathrm{III}})$ plane very close to its vertex; on the contrary, m_{I} and m_{IV} are such that neither the solid nor the fluid phase are fully regenerated. As a result, it leads to a purity of 96.8% for both raffinate and extract. The concentration profiles along the unit change with time, and we define a number of discrete time intervals to capture the dynamics during a switching period at steady state. In this work, time steps of a length of $t^*/8$ have been selected, so that between two switches eight different internal concentration profiles are obtained. The numbering of the columns 1–8 in Fig. 1 refers to their logical position in the SMB, i.e. to their position with respect to the inlet and outlet ports. During a cycle, which consists of eight switches, the logical position of the physical columns labeled A, B, ..., H, changes from right to left, until every physical column has occupied each logical position once. In the first interval of a cycle, between $t = 0$ and $t = t^*$, the logical positions $1, \ldots, 8$ correspond to the physical columns A, ..., H; between $t = t^*$ and $t = 2t^*$ these correspond to B, ..., H, A, and so on until the interval between $t = 7t^*$ and $t = 8t^*$, where they correspond to H, A, ..., G. At time $t = 8t^*$ one cycle has been completed and the sequence starts again.

The defined number of time steps per switch N_t, e.g. in our case $N_t = 8$, divides a switching period into N_t time intervals of the length t^*/N_t. This subdivides a cycle consisting of N_{c} switches (here $N_{\mathrm{c}} = 8$) into $N = N_t N_{\mathrm{c}}$ time steps, i.e. $N = 8 \times 8 = 64$ time steps in our case. A discretization in space is also performed using finite differences: ten grid points per column with $N_{\mathrm{c}} = 8$ corresponds to $N_{\mathrm{g}} = 80$ grid points in all. With this space discretization, from Eq. (1) we generate one ordinary differential equation (ODE) for every species at each grid point, which in our case with two species and $N_{\mathrm{g}} = 80$ leads to a set of 160 ODEs. The $N_t = 8$ internal concentration profiles per switch calculated by the detailed SMB model are used to generate N concentration profiles along the physical columns, each corresponding to one of the 64 discrete time values in the whole cycle. Each of these profiles at the nth time step is constituted of the concentration values $c_{i,g}^{\mathrm{ref}}(n)$, where $i = \mathrm{A, B}$ is the component index, and $g = 1, \ldots, 80$ is the space index. Now, we should consider that the SMB process is described by eight different models in the eight switching time periods within one cycle, since the outlet and inlet streams have different

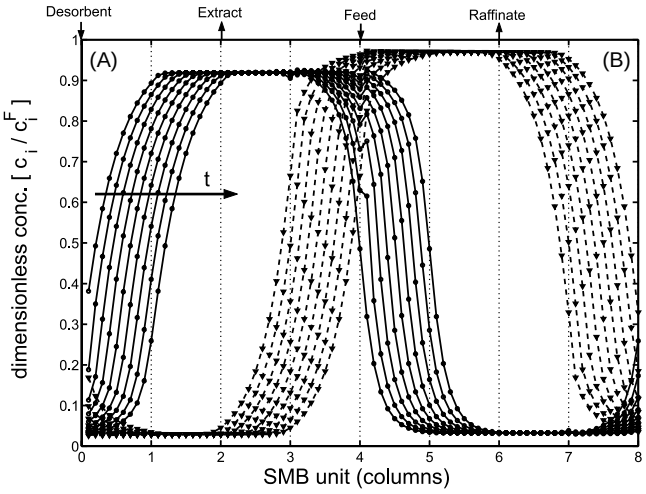

Fig. 3. Propagation of the concentration profile of substance A and B inside the SMB unit showing the time and space discretization of the model.

locations. These are constituted of the same Eqs. (1) and (2), but different node balances (3) to (6). For instance Eq. (3) reads $u_A = u_H + Q_D/A$ in the first switching period of a cycle, whereas it reads $u_B = u_A + Q_D/A$ in the second, and similarly for the other switching periods and the other columns. By linearizing the SMB model with respect to the state and the manipulated variables around each of the 64 reference internal concentration profiles determined above, we obtain 64 different linearized models, each valid for one of the 64 time steps into which a cycle is divided. As an illustration, nine successive reference composition profiles are shown in Fig. 3. Carrying out analytical integration of the ODEs on a time step of length $t^*/8$, yields a set of equations describing the system dynamics that can be recast in matrix form.

$$x_k(n+1) = \mathsf{A}(n)x_k(n) + \mathsf{B}(n)u_k(n), \quad (n = 0, \ldots, N-1) \tag{8}$$

where x and u are vectors, A and B are matrices, and k is the cycle index. The state vector x (of size 160 in this case) is constituted of the deviations from the reference concentration profiles, i.e. $c_{i,g}(n) - c_{i,g}^{\mathrm{ref}}(n)$. The input vector u (of a size equal to the number of manipulated variables, i.e. 4 in our case) consists of the deviations of the internal flow rates with respect to the reference values, i.e. $Q_j(n) - Q_j^{\mathrm{ref}}(n)$ (j = I, II, III, IV), where $Q_j^{\mathrm{ref}} = V(m_j^{\mathrm{ref}}(1-\varepsilon)+\varepsilon)/t^*$ from Eq. (7). The matrices A and B are the operators defining the linearized model, which are calculated at the reference state, which is different at every time step n. The transition from one cycle to the next must satisfy:

$$x_{k+1}(0) = x_k(N) \tag{9}$$

The output vector y is computed from the state vector x as:

$$y_k(n) = \mathsf{C}(n)x_k(n) \tag{10}$$

where C is a matrix. In this case, the output vector has dimension four since it consists of the concentration levels in the extract and raffinate, which are extracted from the state vector by the operator C. For the sake of clarity, in our case the output is constituted of the values $c_{i,20}$ for the extract and $c_{i,60}$ for the raffinate when t is between 0 and t^*, whereas it consists of $c_{i,30}$ and $c_{i,70}$ for t between t^* and $2t^*$, and so on and so forth. The resultant linear time varying (LTV) state space model given by Eqs. (8)–(10) captures not only the time dependent cyclic steady state dynamics but also the hybrid nature of the SMB process.

As the last step, the LTV model is lifted by grouping the input and output values for one cycle, i.e. for time interval $n = 0, \ldots, N$, to obtain a time invariant cycle-to-cycle model [19]. The order of this model is reduced from 160 to 32 by using balanced model reduction [20]. The lifted model is then converted back to an equivalent time-to-time transition model, as proposed by Lee et al. [17]:

$$\tilde{x}_k(n+1) = \tilde{\mathsf{A}}(n)\tilde{x}_k(n) + \tilde{\mathsf{B}}(n)\tilde{u}_k(n), \quad (n = 0, \ldots, N-1) \tag{11}$$

$$\tilde{x}_{k+1}(0) = \tilde{\mathsf{P}}\tilde{x}_k(N) \tag{12}$$

$$y_k(n) = \tilde{\mathsf{C}}(n)\tilde{x}_k(n) \tag{13}$$

The model formulation is similar to Eqs. (8)–(10), but it has to be noted that in the reduced order model the state vector $\tilde{x}$ can no longer be directly related to the individual concentration values at certain grid points in the unit. The reduced order model in this form is then used to predict and optimize the future behavior of the SMB. As a final remark, it is worth mentioning that ideally one can define the period of the process as the time between two switches and obtain a similar model. This will lead to a smaller model and optimization problem. On the other hand, using the global period, i.e. a complete cycle, is preferable because it allows to correct for column-to-column variations and extra-column effects which will repeat itself over the cycles.

3.2. State estimation

As feedback information from the plant the measured concentrations of all components in both extract and raffinate are used. At time n, the computation of the new input variables $\tilde{u}_k(n+1)$ to be implemented at time $n+1$ is started. This requires $\tilde{x}_k(n+1|n)$, i.e. the estimate of the states at time $(n+1)$, $\tilde{x}_k(n+1)$, based on data available at time n. This is determined by a measurement correction step:

$$\tilde{x}_k(n|n) = \tilde{x}_k(n|n-1) + \tilde{\mathsf{K}}(n)[y_{k,\mathrm{measured}}(n) - y_{k,\mathrm{predicted}}(n)], \tag{14}$$

with

$$y_{k,\mathrm{predicted}}(n) = \tilde{\mathsf{C}}(n)\tilde{x}_k(n|n-1), \tag{15}$$

followed by a model forwarding step:

$$\tilde{x}_k(n+1|n) = \tilde{\mathsf{A}}(n)\tilde{x}_k(n|n) + \tilde{\mathsf{B}}(n)\tilde{u}_k(n), \tag{16}$$

where $\tilde{\mathsf{K}}(n)$ is called the filter gain matrix and should be chosen such that the variance of the estimation error is minimized. The resulting estimator is called the Kalman filter and based on the steady-state solution of Riccati difference equation [21]. Detailed description of periodic time varying Kalman filter design and implementation can be found elsewhere [19,22]. It is worth noting that Eq. (16) provides the prediction of the future behavior of the process based on the simplified model and the feedback correction based on the on-line measurements. This is used by the optimizer as described in the following section.

3.3. Optimization

For the optimization we use a moving horizon strategy. We determine how to change the manipulated variables over the *control horizon* such that some objective function evaluated over the *prediction horizon* (≥control horizon) is optimized. We implement the first one of the computed changes and after one time interval we repeat this procedure. Here the control and prediction horizons have been chosen as 1 cycle and 2 cycles, respectively. We seek the minimization of the following objective function, which implies the maximization of production and the minimization of solvent consumption and directly related to the production cost:

$$F = \lambda_1 Q_D^{\text{contr}} - \lambda_2 Q_F^{\text{contr}}, \tag{17}$$

where Q_D^{contr} and Q_F^{contr} are the cumulative solvent consumption and throughput over the control horizon, respectively. λ_1 and λ_2 are the relative weights of the corresponding terms. For our examples we have used $\lambda_1 = 0.25$ and $\lambda_2 = 1.5$. The function F will be referred to as the production cost in the following.

Of course, this problem is subjected to constraints both on the states and the inputs. First of all the purity requirements in the extract and raffinate stream have to be fulfilled; both purity constraints are formulated in terms of the average purity $P_{\text{E}}^{\text{pred}}$ and $P_{\text{R}}^{\text{pred}}$ over the whole prediction horizon. These nonlinear constraints are linearized around the steady-state values at each time step.

$$P_{\text{E}}^{\text{pred}} \geq P_{\text{E}}^{\min} \tag{18}$$

$$P_{\text{R}}^{\text{pred}} \geq P_{\text{R}}^{\min} \tag{19}$$

Beside the constraints on product specifications, constraints on inputs arising from the physics of the process have to be introduced and must be fulfilled during the whole control horizon. The external flow rates must be nonnegative:

$$Q_{\text{R}} = Q_{\text{III}} - Q_{\text{IV}} \geq 0 \tag{20}$$

$$Q_{\text{E}} = Q_{\text{I}} - Q_{\text{II}} \geq 0 \tag{21}$$

$$Q_{\text{F}} = Q_{\text{III}} - Q_{\text{II}} \geq 0 \tag{22}$$

Also the flow rates are limited by the maximum allowable pressure drop resulting in an upper bound for the internal flow rates in section I or III:

$$Q_{\text{I}} \leq Q_{\max} \tag{23}$$

$$Q_{\text{III}} \leq Q_{\max} \tag{24}$$

In addition, the internal flow rates have a physical lower limit of zero.

$$Q_{\text{II}} \geq 0 \tag{25}$$

$$Q_{\text{IV}} \geq 0 \tag{26}$$

Finally, it might be necessary for operational reasons to limit the maximum allowable change in internal flow rates:

$$|\Delta Q_j| \leq \Delta Q_j^{\max} \quad (j = \text{I, II, III, IV}) \tag{27}$$

This guarantees that no excessive pressure changes occur that may damage the column packing.

Note that purities less than the desired, $P_{\text{E}}^{\min}$ and $P_{\text{R}}^{\min}$, may occur during a transient phase, e.g. during plant start-up or during a response to disturbances. Indeed, there may not exist any flow rate sequence over the given control horizon to meet the purity constraints (Eqs. (18) and (19)) that would render the optimization problem infeasible and would cause problems for online applications. Therefore, the purity constraints are relaxed by introducing nonnegative slack variables s_{E} and s_{R}.

$$P_{\text{E}}^{\text{pred}} \geq P_{\text{E}}^{\min} - s_{\text{E}} \tag{28}$$

$$P_{\text{R}}^{\text{pred}} \geq P_{\text{R}}^{\min} - s_{\text{R}} \tag{29}$$

The following cost function together with the constraints (18)–(27) constitute the optimization problem that is formulated to minimize the cumulative solvent consumption and maximize the total productivity over the control horizon,

$$\min_{Q_j(n'), s_{\text{E}}, s_{\text{R}}} [F + \lambda_3 s_{\text{E}} + \lambda_4 s_{\text{R}}] \tag{30}$$

For sufficiently large s_{E}, s_{R} values, the feasibility of the purity constraints is guaranteed. The slack variables are included in the cost function of the optimization problem (Eq. (30)) with large weights, λ_3 and λ_4, so that they will be kept as small as possible ($\lambda_3 = \lambda_4 = 10^3$ in our examples). Generally speaking, the higher the weight of a term, the higher its contribution to the cost and the more it is pronounced in the control behavior. On the other hand, it is worth noticing that one should consider the relative order of magnitude of each term constituting the cost function (Eq. (30)) in order to decide on the weights λ_1 to λ_4. The manipulated variables are the internal flow rates over the control horizon, $Q_j(n')$ with $j = \text{I}, \ldots, \text{IV}$ and $n' = n+1, \ldots, n+N_{\text{contr}}$. N_{contr} corresponds to the number of time steps within the control horizon (64 in our case). The total number of variables for the optimization problem becomes $4N_{\text{contr}} + 2$ slack variables. The structure of the

optimization problem allows other constraints or different performance indices which may be more appropriate for specific applications. The cost function together with the defined constraints constitutes a Linear Program (LP) to be solved at each time step based on the available new measurements. The flow rate sequence obtained as a result of the optimization problem is applied according to a *receding horizon* strategy, i.e. only the first element of the calculated optimal flow rate sequence corresponding to the current time is implemented. A new optimization problem is solved at the next time instance based on the new measurements obtained from the plant output.

With reference to a practical implementation of the control algorithm, it should be noted that the computations needed to solve the optimization problem must be carried out in a time smaller than or equal to the duration of a time step, i.e. $t^*/8 = 60$ s in our work here. It is worth noting that we have used ILOG CPLEX 7.0 as the LP solver and the maximum calculation time to solve the LP was 1.2 s (on a PC with a 3 GHz processor) which is far below the sampling time.

4. Results and discussion

In this section, we present and discuss a number of cases corresponding to different control scenarios, which are meant to assess the performance of the controller. In all simulations the same initial operating point has been selected, i.e. $m_{\mathrm{I}}^{\mathrm{ref}} = 4.0$, $m_{\mathrm{II}}^{\mathrm{ref}} = 2.1$, $m_{\mathrm{III}}^{\mathrm{ref}} = 3.9$ and $m_{\mathrm{IV}}^{\mathrm{ref}} = 2.1$, which is also the one used as a reference for the model linearization. The same lower bound for product purities has been selected for extract and raffinate, i.e. $P_{\mathrm{E}}^{\mathrm{min}} = P_{\mathrm{R}}^{\mathrm{min}} =$ 99%. These initial conditions lead to off-spec production in all examined scenarios. The reason is not the bad choice of the operating point in the $(m_{\mathrm{II}}, m_{\mathrm{III}})$ plane, but rather the wrong values of m_{I} and m_{IV}, which lead to poor regeneration of the adsorbent and the mobile phase, respectively. Poor initial conditions and reference values have been chosen on purpose to better appreciate the performance of the controller. In the following examples, first the cyclic steady state that the SMB reaches in an open loop operation, i.e. without controller action, will be shown; then, the controller is switched on and the attainment of conditions fulfilling product specifications is monitored; later a disturbance is introduced and the SMB operation with on-line control is compared with what happens without the controller.

4.1. Base case

In the first example, the model parameters used by the controller and those of the plant are the same, as far as both the adsorption isotherm and the packing characteristics are concerned. This means that the only source of inaccuracy for the controller model are the numerical approximations introduced, e.g. linearization and model reduction. With reference to Fig. 4, after letting the SMB operate uncontrolled

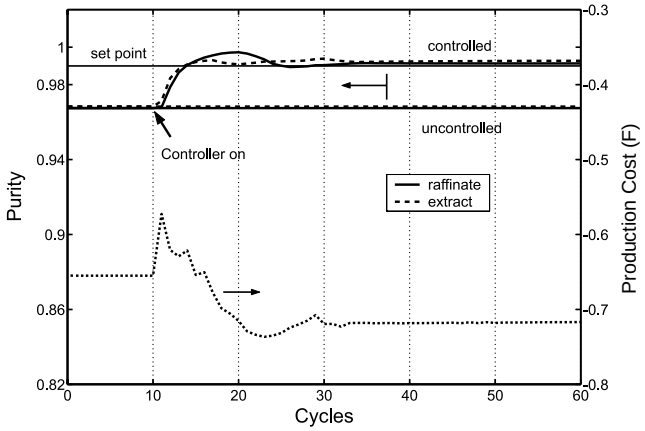

Fig. 4. Outlet purities for the controlled and the uncontrolled SMB and values of the production cost function, F. The plant and controller models have identical parameters.

for 10 cycles, the controller is switched on. It is seen that the controller is able to achieve product specifications from the initial value below 97% in less than five cycles, and stable conditions are achieved about 25 cycles after its activation. Obviously, the uncontrolled plant keeps on operating at the initial off-spec conditions. In Fig. 4 also the production cost F defined by Eq. (17) is shown. It is seen that the controller changes the desorbent and feed flowrate in order to achieve the lowest possible value of F while fulfilling all constraints. When the controller is switched on after cycle 10, it first makes the separation meet process specifications rather quickly, even though this requires a significant increase of F. After the purity specifications are satisfied, the controller adapts the operating conditions to improve the production cost. This continues until about cycle 24 where the purity values approach the lower bound. Therefore, the controller reacts to correct the purities, and this again implies an increase of the production cost. Finally, at about cycle 35, the system settles and the unit operates at a constant value of F, representing the minimum value that the controller was able to achieve while satisfying all the constraints.

In a practical application this behavior would be rather convenient. In fact, the controller first makes sure that the purity specifications are satisfied, which means that the unit produces soon with the desired specifications, and then, on a larger time scale, improves the production cost by minimizing the function, F. If needed one could, of course, change the relative dynamics of these two processes by acting on the values of the coefficients λ_1 and λ_2 in Eq. (17) relative to λ_3 and λ_4 in Eq. (30).

A final remark concerns the accuracy of the developed controller in determining the optimal operating conditions. The on-line optimization is based on an approximate model of the plant, which is obtained linearizing the detailed model, and an estimate of the state of the plant given by a Kalman filter. This implies that the optimization achieved can only approximate the optimal performance that can be identified by carrying out nonlinear off-line optimization using the de-

tailed SMB model, i.e. the plant model. A further consequence relates to the specifications or set points. The output purities calculated by the controller are based on a limited number of data points within a cycle, i.e. output concentration values at N different time instances within a cycle. As a consequence, the purity values calculated and fulfilled by the controller and the purity of the actual plant outputs may show slight differences. This explains the minor differences between the attained purity values and the set values, i.e. $P_{\mathrm{E}}^{\min}$, $P_{\mathrm{R}}^{\min}$. Finally, it is also worth noting that no special effort has been made to optimize the controller performance; this is left for a further investigation.

4.2. Model/plant mismatch: adsorption isotherms

A typical situation in SMB chromatography is that there is some uncertainty about the parameters of the adsorption isotherm describing the system under consideration. This may be due to several reasons, from measurement errors and uncertainties during isotherm characterization, to packing material degradation, or due to improper temperature control of the chromatographic columns during operation. Although this problem is certainly more significant in the case of non-linear isotherms for multi-component systems, it is worth considering it also in the case of linear binary isotherms. Therefore, in the second example illustrated in Fig. 5 we consider a model plant mismatch regarding Henry's constants, H_{A} and H_{B}, where the "real" plant values are 4.4 and 2.3, i.e. 10% and 15% larger than the values used by the controller, respectively. This implies that the plant operates with a selectivity $S = 1.9$, i.e. 4% less than the nominal one. Such discrepancy leads to very poor purity performance when the plant is operated without controller for the given initial conditions. As in the case illustrated in Fig. 4, the controller is switched on after 10 cycles; the SMB meets the product specifications within eight cycles, and reaches a

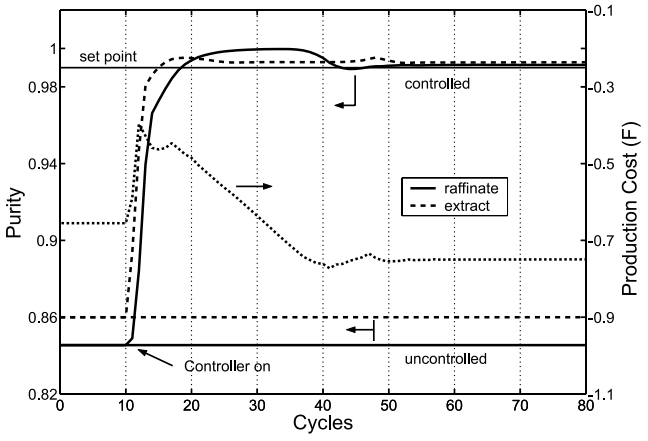

Fig. 5. Outlet purities for the controlled and the uncontrolled SMB and values of the production cost function, F. The Henry's constants of the model plant are larger than in the controller model ($\Delta H_{\mathrm{A}} = +10\%$, $\Delta H_{\mathrm{B}} = +15\%$).

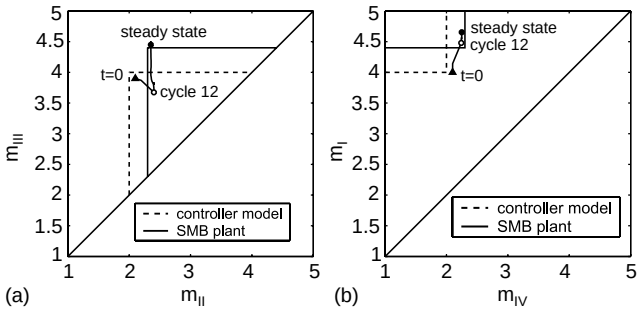

Fig. 6. Trajectory of the operating point (a) in the $(m_{\mathrm{II}}, m_{\mathrm{III}})$ plane and (b) in the $(m_{\mathrm{I}}, m_{\mathrm{IV}})$ plane compared to the complete separation and regeneration regions, respectively for the controlled separation shown in Fig. 5. m values are averaged for each cycle.

cyclic steady state about forty cycles later. Also the production cost function F behaves similarly as in the base case. First, the purity specifications are fulfilled at the expense of an increase of F, then the performance is optimized and F decreases, until the purity hits the lower bound. This causes a small increase in F, but then the optimal separation performance is attained and the operation continues with a constant value of F.

In Fig. 6, the control action is analyzed in terms of operating parameters, i.e. of the flow rate ratios m_j. Fig. 6a refers to m_{II} and m_{III}, whereas Fig. 6b refers to m_{IV} and m_{I}. In the former the complete separation regions defined as $H_{\mathrm{B}} \leq m_{\mathrm{II}} \leq m_{\mathrm{III}} \leq H_{\mathrm{A}}$ are shown [8]; the one with solid boundaries applies to the "real" plant, whereas that with dashed boundaries applies to model available to the controller. In Fig. 6b, the regions of complete regeneration defined by $m_{\mathrm{I}} \geq H_{\mathrm{A}}$ and $m_{\mathrm{IV}} \leq H_{\mathrm{B}}$ are shown, using the same convention as in Fig. 6a. In the frame of equilibrium theory, i.e. assuming negligible axial dispersion and mass transfer resistance, high purity separations can be achieved only for operating points located inside the complete separation and regeneration regions shown in Fig. 6a and b, respectively. It can be readily observed that the initial operating point is inside the complete separation region of the controller model in the $(m_{\mathrm{II}}, m_{\mathrm{III}})$ plane and slightly outside its complete regeneration region in the $(m_{\mathrm{IV}}, m_{\mathrm{I}})$ plane. However, it is outside both regions for the SMB plant, which explains the poor initial purity values in Fig. 5. As soon as the controller is switched on, the operating point moves rapidly towards the correct regions for the plant and enters them after only 2 cycles, i.e. at cycle 12. The operating conditions are adjusted in order to meet first the purity requirements, which occurs after only 8 cycles, and then to improve performance, which requires more time. The operating point moves towards the vertex of the triangle region in Fig. 6a and to that of the rectangular region in Fig. 6b (both with solid boundaries, i.e. those applying to the plant). The final operating point is reached about 40 cycles after activation of the controller and is close to the equilibrium theory optimum, which is located

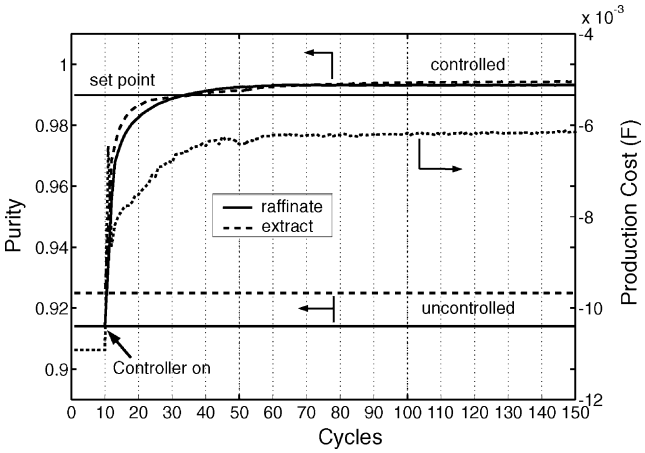

Fig. 7. Comparison of the SMB outlet purities in the controlled and uncontrolled case. The model plant has the following packing porosity values: $\varepsilon_A = 0.6300$, $\varepsilon_B = 0.8505$, $\varepsilon_C = 0.8505$, $\varepsilon_D = 0.7380$, $\varepsilon_E = 0.4500$, $\varepsilon_F = 0.5220$, $\varepsilon_G = 0.5895$, $\varepsilon_H = 0.4095$, which give a mean porosity that is 10% smaller than that of the controller model. Number of theoretical plates: $N_p = 100$ in the controller model, $N_p = 20$ in the plant model.

at the vertex of both the triangular (complete separation) and rectangular (complete regeneration) regions [8]. This is because high efficiency columns are used in this example, i.e. columns with $N_p = 100$. If lower efficiency columns had been considered, the final operating point would have been further away from the theoretical vertex [9].

4.3. Model/plant mismatch: column packing

Another critical issue, particularly in SMB operation, has to do with column packing, which should in principle be exactly the same in all SMB columns, but may exhibit more or less significant differences. Moreover, column efficiency may be difficult to assess, particularly under overload conditions, or may change during operation due to aging of the packing. The example illustrated in Fig. 7 addresses these issues, by considering a situation where the packing parameters of the plant differ from the nominal ones used by the controller model. In particular, we assume that the average column void fraction in the plant is $\varepsilon = 0.63$, i.e. 10% less than in the model, and that the values for the individual columns differ in a range of ±35% ($\varepsilon_A = 0.6300, \varepsilon_B = 0.8505, \varepsilon_C = 0.8505, \varepsilon_D = 0.7380, \varepsilon_E = 0.4500, \varepsilon_F = 0.5220, \varepsilon_G = 0.5895, \varepsilon_H = 0.4095$). In addition, the efficiency of the plant is significantly lower than that of the model; the number of theoretical plates is 20 instead of 100. These deviations might be extreme, but they provide a significant challenge to the robustness and capabilities of the controller. As in the case considered in the previous section, Fig. 7 shows that the controller is able to meet the product specifications, even though its action is more sluggish and about 25 and 80 cycles are needed to reach the purity set point and performance stabilization, respectively.

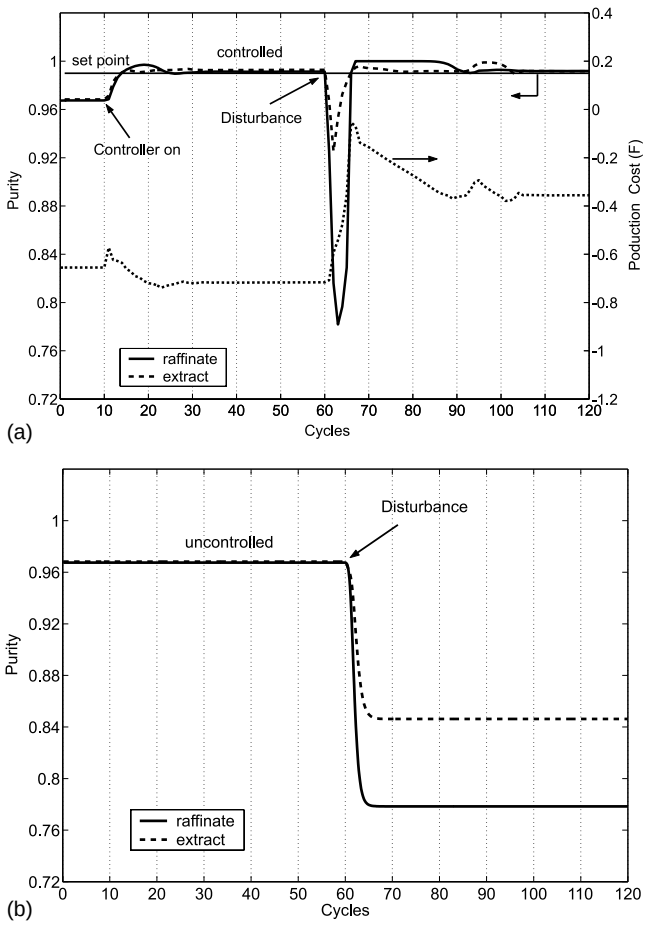

Fig. 8. Outlet purities for the controlled and the uncontrolled SMB and values of the production cost function, F. The controller is switched on after reaching the steady-state and a step disturbance in Henry's constants takes place at cycle 60.($\Delta H_A = -15\%$, $\Delta H_B = +15\%$).

4.4. Step disturbance

The next two examples analyze how the controller copes with disturbances that perturb the stationary operation of the SMB unit achieved as described in Section 4.1 and illustrated in Fig. 4. In the first case we consider a sudden temperature change, which leads to a step change of the model parameters characterizing the plant operation, e.g. the adsorption isotherm parameters. Such a situation is addressed in Fig. 8, where it is assumed that after 60 cycles of 'base case' operation (see Fig. 4) Henry's constants of the plant change by ±15%, i.e. they attain the new values $H_A = 3.4$ and $H_B = 2.3$, corresponding to a much reduced selectivity $S = 1.5$, i.e. 25% less than the model value. Such a disturbance leads to a dramatic, unacceptable drop of product purity in the case of the uncontrolled operation, as shown in Fig. 8b. On the other hand, in the case of the controlled SMB operation, the purity drops immediately after the disturbance, but then the controller is able to bring the operation back to fulfill the product specifications in a rather short time, i.e. in about six cycles as seen in Fig. 8a. In the same

figure we also see that the production cost, after the product specifications are satisfied, decreases continuously and reaches its minimum value after about forty five cycles. This result shows that even in the presence of a rather dramatic, sudden disturbance, the controller is able to limit the amount of off-spec product that has to be discarded or recycled, and to optimize the separation.

4.5. Ramp disturbance

In this example, we consider a similar disturbance as the one analyzed in the previous section, which manifests itself gradually over a finite time interval. We assume that a change of Henry's constants takes place linearly with time. In this case H_A increases from 4 to 4.4, and H_B from 2 to 2.3 in a period of time corresponding to fifty cycles starting from fifty cycles after the controller is switched on. We expect that the final SMB regimes in the controlled and in the uncontrolled case will be similar to those illustrated in Fig. 8, but that the system transient will be different. The situation considered here is representative of cases where there is a slow aging of the stationary phase, thus modifying gradually the retention behavior of the species to be separated, or where the SMB unit undergoes periodic, e.g. daily, temperature variations.

The results obtained are illustrated in Fig. 9. It is seen that starting at cycle 60 the uncontrolled plant exhibits a slow drift towards very low purity values. On the contrary, the controller is able to keep the purity of both extract and raffinate within specifications at all times during and after the change of adsorption parameters. Fig. 10 shows how the operating point moves with respect to the actual separation region in the (m_{II}, m_{III}) plane, until optimal operating conditions are reached. The three triangles show the complete separation regions corresponding to values of Henry's constant values prevailing at the point in time (cycle number) indicated in the same figure, while the symbols indicate the

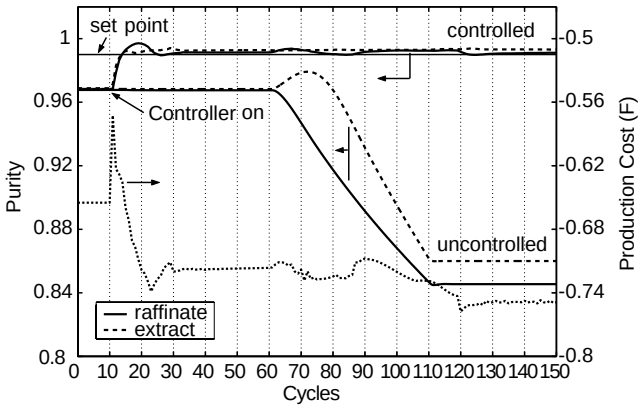

Fig. 9. Outlet purities for the controlled and the uncontrolled SMB and values of the production cost function, F. The controller is switched on after reaching the steady-state and a ramp disturbance in Henry's constants is applied between cycle 60 and cycle 110. ($\Delta H_A = +10\%$, $\Delta H_B = +15\%$).

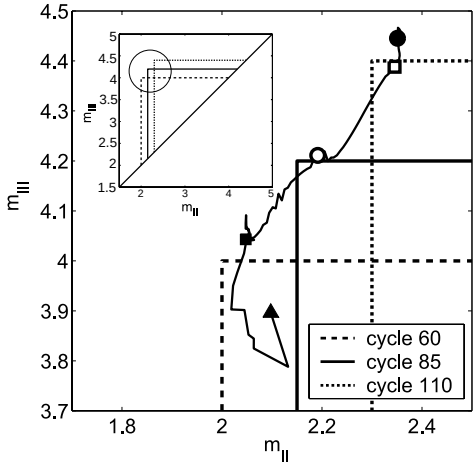

Fig. 10. Trajectory of the operating point and of the corresponding complete separation region in the (m_{II}, m_{III}) plane during the controlled separation shown in Fig. 9. The symbols correspond to the time $t = 0$ (▲), cycle 60 (■), cycle 85 (○), cycle 120 (□) and the steady state (●). m values are averaged for each cycle.

operating conditions of the controlled plant at the same time. It is seen that these points follow rather closely the vertex of the triangle as expected based on triangle theory. In addition, one can observe that during the ramp disturbance, the distance of the vertex of the complete separation region from the diagonal, which according to triangle theory is proportional to the feed flow rate, increases. This indicates that the function F can achieve better values, since in our case the relative weight given to the feed flow rate, λ_2 in Eq. (17), is much larger than that of the desorbent flow rate, λ_1. As shown in Fig. 9, better values of F, where the value decreases from -0.71 before the disturbance to -0.75 after it, are in fact found by the controller. This is confirmed by the results shown in Fig. 8 for the step disturbance. In that case the vertex of the complete separation region after the disturbance is closer to the diagonal, and in fact the controller reaches an optimal value for the production cost at the end of the disturbance which is worse than before, i.e. -0.35 instead of -0.70. These observations support the fact that the controller is actually able to identify the optimal operating conditions or at least to move in the right direction.

5. Conclusions

An optimization based adaptive control strategy for SMBs using repetitive model predictive control has been developed. The controller uses a simplified, approximate model of the real plant. The strength of this controller is its effectiveness also when the simplified model is not accurate, e.g. where only approximate thermodynamic data, i.e. Henry's constants, are available. The performance of the controller has been tested thoroughly under extreme model/plant mismatch conditions or large disturbances of various origin; we consider all the results shown here rather encouraging. They

indicate that the developed approach provides a promising tool to develop a fully automatized SMB unit. In future works the behavior of the controller will be tested for other likely SMB disturbances, e.g. fluctuating flow rates, as well as for separations under nonlinear competitive adsorption conditions or with SMBs with a smaller number of columns.

6. Nomenclature

$\mathsf{A}, \mathsf{B}, \mathsf{C}$	state space model matrices
$\tilde{\mathsf{A}}, \tilde{\mathsf{B}}, \tilde{\mathsf{C}}, \tilde{\mathsf{P}}$	state space model matrices after model reduction
A	column cross-section (cm^2)
c	concentration (g/l)
D	apparent axial dispersion coefficient (cm^2/s)
F	production cost
H	Henry's constant
$\tilde{\mathsf{K}}$	Kalman filter gain matrix
k	cycle index
L	column length (cm)
m	flow rate ratio
N	number of time steps per cycle
N_p	number of theoretical plates
N_c	total number of columns in the SMB
N_g	total number of grid points in the SMB
N_t	number of time steps during a switching period
n	time step index
P	purity
Q	volumetric fluid flow rate (ml/min)
q^*	adsorbed phase concentration (g/l)
S	selectivity (-)
s	slack variable (-)
t	time (s)
t^*	switch time (s)
u	vector of manipulated variables
v	internal flow rate (ml/min)
V	volume of one column (ml)
x	state vector
$\tilde{x}$	state vector of reduced order model
y	vector of output concentrations
z	axial coordinate (cm)

Greek letters

ε	bed void fraction
λ	weighting factor in cost function

Subscripts and superscripts

$A, \ldots, H$	index for physical columns
contr	control horizon
D	desorbent
E	extract
F	feed
g	space index (grid point number)
h	column position index ($h = 1, \ldots, 8$)
I/O	inlet/outlet stream
in	column inlet
i	component index ($i = \mathrm{A}, \mathrm{B}$)
j	section index, ($j = \mathrm{I}, \ldots, \mathrm{IV}$)
max	maximum
min	minimum
out	column outlet
pred	predicted
R	raffinate
ref	reference value

Acknowledgements

The authors are grateful to Prof. Jay H. Lee and Prof. Hyun-Kuh Rhee, for helpful discussions. The support of ETH Zurich through grant TH-23′/00-1 is gratefully acknowledged.

References

[1] M. Juza, O. Di Giovanni, G. Biressi, M. Mazzotti, V. Schurig, M. Morbidelli, J. Chromatogr. A 813 (1998) 333–347.
[2] R.M. Nicoud, in: G. Subramanian (Ed.), Bioseparation and Bioprocessing, Wiley–VCH, New York, 1998.
[3] E. Francotte, J. Richert, M. Mazzotti, M. Morbidelli, J. Chromatogr. A 796 (1998) 239–248.
[4] M. Juza, M. Mazzotti, M. Morbidelli, Trends Biotechnol. 18 (2000) 108–118.
[5] O. Ludemann-Hombourger, R.M. Nicoud, M. Bailly, Sep. Sci. Technol. 35 (2000) 1829.
[6] O. DiGiovanni, M. Mazzotti, M. Morbidelli, F. Denet, W. Hauck, R.M. Nicoud, J. Chromatogr. A 919 (2001) 1.
[7] S. Abel, M. Mazzotti, M. Morbidelli, J. Chromatogr. A 944 (2002) 23.
[8] M. Mazzotti, G. Storti, M. Morbidelli, J. Chromatogr. A 769 (1997) 3.
[9] C. Migliorini, A. Gentilini, M. Mazzotti, M. Morbidelli, Ind. Eng. Chem. Res. 38 (1999) 2400.
[10] E. Kloppenburg, E.D. Gilles, J. Process Control 9 (1999) 41.
[11] P. Marteau, G. Hotier, N. Zanier-Szydlowski, A. Aoufi, F. Cansell, Process Control Qual. 6 (1994) 133.
[12] K.U. Klatt, F. Hanisch, G. Dünnebier, J. Process Control 12 (2002) 203.
[13] H. Schramm, S. Grüner, A. Kienle, E.D. Gilles, in: Proceedings of European Control Conference 2001, Porto, Portugal, 2001, pp. 2528–2533.
[14] C.E. Garcia, D.M. Prett, M. Morari, Automatica 25 (3) (1989) 335.
[15] A. Bemporad, M. Morari, Lecture Notes in Control and Information Sciences 245 (1999) 207.
[16] S. Natarajan, J.H. Lee, Comput. Chem. Eng. 24 (2000) 1127.
[17] J.H. Lee, S. Natarajan, K.S. Lee, J. Process Control 11 (2001) 195.
[18] G. Guiochon, S. Golshan-Shirazi, A.M. Katti, Fundamentals of Preparative and Nonlinear Chromatography, Academic Press, 1994.
[19] G. Erdem, S. Abel, M. Morari, M. Mazzotti, M. Morbidelli, J.H. Lee, Ind. Eng. Chem. Res. 43 (2004) 405.
[20] MATLAB®, Control System Toolbox, The MathWorks Inc.
[21] R.E. Kalman, Trans. ASME J. Basic Eng. 82 (1960) 35.
[22] K.S. Lee, J.H. Lee, in: Z. Bien, J. Xu (Eds.), Iterative Learning Control: Analysis, Design, Integration and Applications, Kluwer Academic Publishers, 1998.